

The pulse tube and the pendulum

G. W. Swift and S. Backhaus

Condensed Matter and Thermal Physics Group, Los Alamos National Laboratory, Los Alamos, New Mexico 87545

(Received 2 June 2009; revised 17 August 2009; accepted 20 August 2009)

An inverted pulse tube in which gravity-driven convection is suppressed by acoustic oscillations is analogous to an inverted pendulum that is stabilized by high-frequency vibration of its pivot point. Gravity acts on the gas density gradient arising from the end-to-end temperature gradient in the pulse tube, exerting a force proportional to that density gradient, tending to cause convection when the pulse tube is inverted. Meanwhile, a nonlinear effect exerts an opposing force proportional to the square of any part of the density gradient that is not parallel to the oscillation direction. Experiments show that convection is suppressed when the pulse-tube convection number $N_{\text{ptc}} = \omega^2 a^2 \sqrt{\Delta T / T_{\text{avg}}} / [g(\alpha D \sin \theta - L \cos \theta)]$ is greater than 1 in slender tubes, where ω is the radian frequency of the oscillations, a is their amplitude, ΔT is the end-to-end temperature difference, T_{avg} is the average absolute temperature, g is the acceleration of gravity, L is the length of the pulse tube and D is its diameter, α is about 1.5, and the tip angle θ ranges from 90° for a horizontal tube to 180° for an inverted tube. Theory suggests that the temperature dependence should be $\Delta T / T_{\text{avg}}$ instead of $\sqrt{\Delta T / T_{\text{avg}}}$. © 2009 Acoustical Society of America. [DOI: 10.1121/1.3238156]

PACS number(s): 43.35.Ud, 43.25.Ts, 43.28.Py [RR]

Pages: 2273–2284

I. INTRODUCTION

Rigid pendula exhibit many interesting phenomena,¹ including dynamic stabilization: If the pivot point of a rigid pendulum is vibrated at high enough frequency and high enough amplitude, the pendulum tends to align with the vibration axis, and the pendulum can stand inverted, seeming to defy gravity. The equation of motion can be derived with the simple approach of Blitzer.² Let the x and y directions, the angle θ of the pivot-point vibration relative to gravity g , and the angle $\phi(t)$ of the pendulum relative to gravity be defined as shown in Fig. 1(a), and let m be the mass of the pendulum's bob and L be the length of its rod. The positions $x(t)$ and $y(t)$ of the pendulum's bob are given by

$$x = a \sin \theta \cos \omega t + L \sin \phi, \quad (1)$$

$$y = -a \cos \theta \cos \omega t - L \cos \phi, \quad (2)$$

when the pivot point is forced to vibrate sinusoidally with amplitude a and radian frequency ω . The equation of motion for the bob can be written as

$$F_x = m\ddot{x}, \quad F_y - mg = m\ddot{y}, \quad (3)$$

where the F 's are the two components of force exerted by the rod on the bob and the overdots represent time derivatives. By Newton's third law, the bob exerts force $-\vec{F}$ on the rod, applied at the end of the rod attached to the bob. The torque on the rod about the pivot point due to $-\vec{F}$ must be zero, because this massless rod has zero moment of inertia, I_{rod} . Thus

$$-LF_x \cos \phi - LF_y \sin \phi = I_{\text{rod}} \ddot{\phi} = 0. \quad (4)$$

Combining these four equations by eliminating x , y , F_x , and F_y yields the equation of motion for the pendulum angle ϕ as follows:

$$\ddot{\phi} = -(g/L) \sin \phi + \omega^2 (a/L) \sin(\theta - \phi) \cos \omega t. \quad (5)$$

For $0 < \phi < 180^\circ$, the torque applied by gravity that tends to decrease ϕ is apparent in Fig. 1(a) and Eq. (5). The time-averaged torque caused by the pivot-point vibration, tending to align ϕ with the vibration, is not so apparent in Fig. 1(a) or Eq. (5), but Fig. 1(b) helps explain the mechanism, if the vibration is exaggerated and gravity is neglected.¹ The figure shows the pendulum at two extremes j and k of its motion under this exaggerated circumstance. At j , the acceleration of the pivot point causes a large, positive $\dot{\phi}$, without much acceleration of the bob. At k , the acceleration of the pivot point causes the bob to accelerate parallel to the vibration direction, with only a small, negative $\dot{\phi}$. The net effect on ϕ is positive, causing the pendulum to tend to align with the vibration. In other words, the time-averaged torque tending to align ϕ with the vibration is proportional to the product of the amplitude of the angular vibration, $\phi_k - \phi_j$, and how strongly the torque caused by the vibration varies with ϕ .

For decades, quantitative analysis of Eq. (5) when $\omega^2 \gg g/L$ has appeared as an exercise in textbooks on classical mechanics, such as Ref. 3 for $\theta=180^\circ$ and $\theta=90^\circ$ and Ref. 4 for $\theta=180^\circ$. Extended to arbitrary θ , the analysis shows that the dimensionless number

$$N_{\text{pendulum}} = \frac{\omega^2 a^2}{gL} \quad (6)$$

determines the simple pendulum's behavior for slow time scales, i.e., time scales $\gg 1/\omega$. For $N_{\text{pendulum}} > 4$, the pendulum can be stably held up for any θ . For $1 < N_{\text{pendulum}} < 4$, it can be stably held up only if the pivot-point's vibration is close enough to vertical (i.e., close enough to either $\theta=0^\circ$ or $\theta=180^\circ$, which are equivalent). For $N_{\text{pendulum}} < 1$, the pendulum cannot be stably inverted for any θ . (The details of this

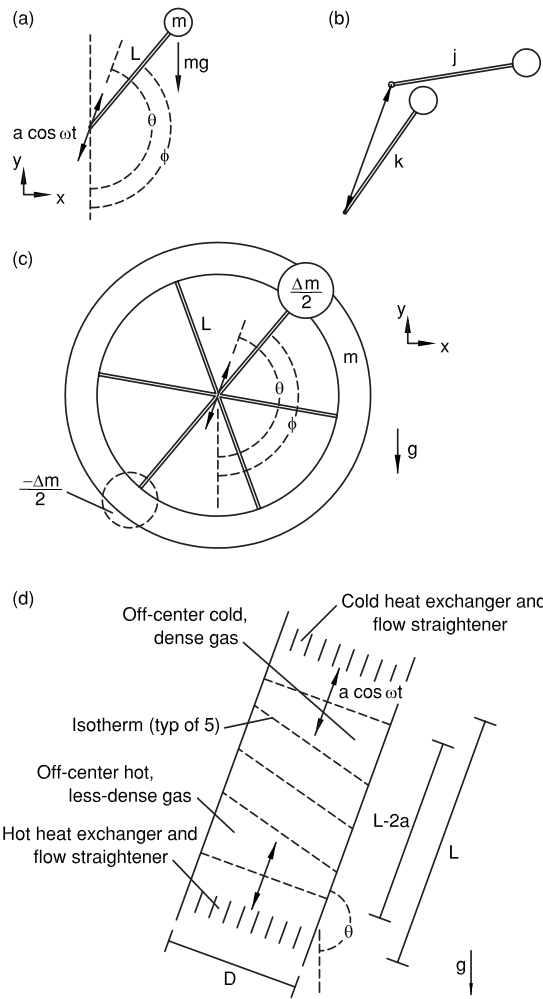


FIG. 1. (a) An inverted, rigid pendulum whose support is vibrated at a high enough frequency and amplitude can be stabilized against falling over. Relative to gravity, which points in the $-y$ direction, θ gives the angle along which the vibrations occur, and $\phi(t)$ gives the angle of the pendulum. (b) Consideration of an exaggerated situation, in which the amplitude of the pivot-point oscillation is not small compared with the length of the pendulum's rod, illustrates the stabilization mechanism. (c) An out-of-balance ring that is vibrated at its central pivot point behaves similarly, due to the same mechanism, but described by slightly more complicated mathematics. (d) An inverted pulse tube whose gas is oscillated at a high enough frequency and amplitude can be stabilized against natural convection, because of a similar mechanism. The double-headed arrows show the peak-to-peak amplitude $2a$ of the acoustic oscillation, assumed to carry all isotherms. Ideally, the central slug of gas, whose length is $L-2a$, would experience no gravity-driven convection.

analysis are omitted here, because similar details are presented in the next paragraph and in Sec. II.)

A more complicated pendulum sets the stage well for analysis of the pulse tube in Sec. II. Figure 1(c) shows a ring of radius L and mass m , supported from its central pivot point by massless spokes. The mass m is uniformly distributed around the ring, except for an out-of-balance part $\Delta m/2$, which has been removed from location $-\phi$ and added to location $+\phi$. The pivot point is forced to vibrate sinusoidally along a line at angle θ from the vertical, with amplitude a and angular frequency ω , as for the simple pendulum considered above, and the analysis again begins by following Blitzer's approach.² The coordinates of the "positive" mass at $+\phi$ and the "negative" mass at $-\phi$ are written down, as are

equations of motion for these two masses. The torque exerted on the ring by its contact with the two out-of-balance masses is set equal to $I_{\text{ring}}\ddot{\phi}$, where $I_{\text{ring}}=mL^2$ is the ring's moment of inertia. Eliminating the forces and coordinates yields an equation of motion for the angle $\phi(t)$,

$$mL^2\ddot{\phi} = -\Delta mgL \sin\phi + \Delta m\omega^2 aL \sin(\theta - \phi)\cos\omega t \quad (7)$$

$$\equiv \tau_{\text{grav}} + \tau_{\text{vib}}, \quad (8)$$

where the right-hand side can be interpreted as the sum of a torque due to gravity and a torque due to the vibration of the pivot. References 3 and 4 show that the pendulum angle ϕ should be written as the sum of slow and fast parts

$$\phi = \phi_{\text{slow}} + \phi_{\text{fast}} \cos\omega t, \quad (9)$$

when $\omega^2 \gg \Delta mg/mL$. Using Taylor-series expansions

$$\tau = \tau|_{\phi_{\text{slow}}} + \left. \frac{\partial \tau}{\partial \phi} \right|_{\phi_{\text{slow}}} \phi_{\text{fast}} \cos\omega t \quad (10)$$

for both terms on the right-hand side of Eq. (7) and time averaging confirms that there was no need for a $\sin\omega t$ term in Eq. (9) and it generates two equations: a "fast" equation from the $\cos\omega t$ terms and a "slow" equation from terms with nonzero time-averages,

$$\phi_{\text{fast}} = -\frac{\Delta m a}{m L} \sin(\theta - \phi_{\text{slow}}), \quad (11)$$

$$mL^2\ddot{\phi}_{\text{slow}} = -\Delta mgL \sin\phi_{\text{slow}} + \frac{(\omega a \Delta m)^2}{4m} \sin(2\theta - 2\phi_{\text{slow}}). \quad (12)$$

If this pendulum can be stably inverted, then $\ddot{\phi}_{\text{slow}}=0$ and setting the right-hand side of Eq. (12) equal to zero must yield a solution for ϕ_{slow} . Whether such a solution exists, and its value, depends on the ratio of the coefficients of the two terms on the right (dropping the factor of 4 for simplicity),

$$N_{\text{ring}} = \frac{\omega^2 a^2 \Delta m}{gL m}. \quad (13)$$

It is interesting how many effects combine to put Δm and $(\Delta m)^2/m$ in the two terms on the right-hand side of Eq. (12), and hence to put $\Delta m/m$ in Eq. (13). The left-hand side of Eq. (12) is the moment of inertia times the slow angular acceleration, so the right-hand side must be the slow torque. The first term on the right-hand side shows gravity applying torque proportional to the unbalanced mass Δm , with the mass $\Delta m/2$ trying to drop down on the right and the negative mass $-\Delta m/2$ trying to float up on the left, both applying clockwise torques in Fig. 1(c). The second term on the right-hand side, which represents the time-averaged torque tending to align the unbalanced axis of the ring with θ , arises from the mechanism illustrated in Fig. 1(b), i.e., the time-averaged product of $\partial \tau_{\text{vib}}/\partial \phi$ and ϕ_{fast} in Eq. (10), where τ_{vib} is the vibration torque given by the second term in Eq. (7). The unbalanced mass Δm appears in the numerator of ϕ_{fast} in Eq. (11) because it is responsible for τ_{vib} through the mechanism shown in Fig. 1(b). The ring mass m appears in the denomi-

nator of ϕ_{fast} in Eq. (11) because the ring's moment of inertia resists the fast torque. Finally, $\partial\tau_{\text{vib}}/\partial\phi$ retains the mass dependence of τ_{vib} itself, namely, Δm . Overall, N_{ring} represents the angle-independent part of the ratio of the time-averaged alignment torque [proportional to $(\Delta m)^2/m$] to the gravitational torque (proportional to Δm).

This paper explores the hypothesis that a similar mechanism is responsible for suppressing natural convection in the gas in a tube with an axial temperature gradient, when the gas oscillates axially at high enough frequency and amplitude. As shown in Fig. 1(d) for such a tube with its cold end higher than its hot end, gravity tends to pull the dense gas near the cold end to one side and down, pushing the less-dense gas near the hot end to the other side and up. This puts the center of mass of the gas below the tube's centerline. The vibration can then exert a time-averaged torque on the entire body of gas, via time-averaged oscillating forces on this off-center center of mass, in a process analogous to that shown in Fig. 1(b). This torque opposes that of gravity and can balance it, preventing convection.

The gas in a pulse tube experiences such axial oscillations and supports such an axial temperature gradient. The pulse tube, a vital component of cryogenic pulse-tube refrigerators,⁵ is a smooth-walled tube without internal structures, bounded on both ends by flow straighteners and heat exchangers through which gas flows easily. Its purpose is to transmit acoustic power through the gas from the cold end to the hot end with minimal heat leak from the hot end to the cold end. The lack of internal structure generally makes low-loss transmission of acoustic power easy, but makes heat-leak minimization challenging. The peak-to-peak volumetric stroke of the moving gas is always less than the volume of the gas in a pulse tube. Ideally, one imagines a perfectly thermally stratified slug of gas, whose volume is the difference between the tube volume and the volumetric stroke, oscillating axially in the tube and remaining entirely inside the tube at all times, conducting only a little heat from hot to cold, without any accompanying convection. However, several heat-transfer mechanisms can disturb this ideal picture, carrying much more heat than would be carried by conduction alone, unless attention is paid to minimizing each one of them. One such heat-transfer mechanism—natural convection due to gravity acting on density gradients in the gas, the subject of this paper—is known to occur commonly in low-frequency pulse-tube refrigerators, but it is also known that such convection is often reduced or absent in high-frequency pulse-tube refrigerators.⁶⁻⁸

Our motivation for this work arose in the context of pulse-tube refrigerators and thermoacoustic engines, sometimes coupled, in which convectively stable orientation of the tubes relative to gravity was inconvenient and an accurate understanding of the suppression of convection by high-frequency oscillations was desired. In thermoacoustic-Stirling hybrid engines⁹ and cascade thermoacoustic engines,¹⁰ the tubes that transmit acoustic power across a temperature difference while minimizing heat leak are called thermal-buffer tubes. They generally carry acoustic power from a hot temperature to ambient temperature, while pulse tubes carry acoustic power from a cold temperature to ambi-

ent temperature. But even in pulse-tube refrigerators, these tubes are sometimes called thermal-buffer tubes. For brevity in this paper, all such tubes are referred to as pulse tubes, and their end temperatures are labeled as hot and cold.

Below, theoretical arguments (Sec. II) and experimental evidence (Sec. III) are presented to show that

$$N_{\text{ptc}} = \frac{\omega^2 a^2}{g(\alpha D \sin \theta - L \cos \theta)} \left(\frac{\Delta T}{T_{\text{avg}}} \right)^\beta \quad (14)$$

is a useful and plausible choice of dimensionless group for characterizing this phenomenon in pulse tubes of low-aspect ratio D/L . As above, ω is the radian frequency of the oscillation, a is its displacement amplitude, and g is the acceleration of gravity; D is the pulse-tube diameter and L is its length, ΔT is the end-to-end temperature difference, and T_{avg} is the average temperature. The tip angle θ is taken to be zero in the vertical, gravitationally stable orientation, and this equation is only valid for $90^\circ \leq \theta \leq 180^\circ$ (where $\cos \theta \leq 0$, so both terms in the denominator are non-negative). The parameter α is a fitting parameter discussed below, experimentally found to be about 1.5, and experiment shows that β is close to 1/2 while theory suggests $\beta=1$.

II. THEORY

An extensive literature describes the interaction between rapid vibration and steady convection in fluids, in the framework of the Boussinesq approximation, namely, that density variations due to temperature variations are small and density variations due to pressure variations are zero. This literature is reviewed and its foundations are succinctly summarized by Gershuni and Lyubimov.¹¹ After writing the hydrodynamic and thermal variables as the sum of fast variations at the vibration frequency and slow variations, they derive time-averaged equations of motion for the slow variables similar in spirit to Eq. (12) above, showing that fast vibrations effectively add a time-averaged body force to the fluid, whose magnitude and direction depend on the magnitude and direction of the vibration velocity and the fluid's temperature-gradient vector field. For steady state with negligible convection, their Eqs. (1.100) and (1.101) give the conditions for balance between gravity- and vibration-induced forces

$$\text{Ra} \vec{\nabla} T \times \hat{g} + \text{Ra}_{\text{vib}} \vec{\nabla}(\vec{w} \cdot \hat{n}) \times \vec{\nabla} T = 0, \quad (15)$$

$$\vec{\nabla} \cdot \vec{w} = 0, \quad (16)$$

$$\vec{\nabla} \times \vec{w} = \vec{\nabla} T \times \hat{n}, \quad (17)$$

where \hat{g} and \hat{n} are unit vectors in the directions of gravity and the vibration, respectively, T is the time-averaged temperature, \vec{w} is the solenoidal part of $T\hat{n}$, and the ordinary Rayleigh number Ra and the vibrational Rayleigh number Ra_{vib} are given by

$$\text{Ra} = \frac{l^3 g \Delta T_{\text{char}}}{\nu \kappa T_{\text{char}}}, \quad (18)$$

$$\text{Ra}_{\text{vib}} = \frac{(\omega a l \Delta T_{\text{char}})^2}{2 \nu \kappa T_{\text{char}}^2}, \quad (19)$$

with l a characteristic length of the boundary of the fluid, ΔT_{char} a characteristic temperature difference, T_{char} a characteristic temperature, ν a characteristic kinematic viscosity, and κ a characteristic thermal diffusivity. In Eqs. (18) and (19), we have set the thermal expansion coefficient of Ref. 11 equal to $1/T$, as appropriate for an ideal gas. Evident from Eq. (15), the existence of a steady state without convection depends on the ratio of Ra_{vib} and Ra ,

$$\frac{\omega^2 a^2 \Delta T_{\text{char}}}{g l T_{\text{char}}}. \quad (20)$$

Although derived in the context of the Boussinesq approximation, which is not really applicable to pulse tubes, this expression suggests most of the functional dependences that are displayed in Eq. (14), most of which are confirmed in the experiments described below. Presumably, numerical analysis based on Eqs. (15)–(17) could show whether the pulse-tube's length L , its diameter D , or some combination of those variables is best used for the characteristic length l , and could find the tip-angle dependence of vibrational suppression of convection in a pulse tube.

A high vibrational Rayleigh number tends to align density gradients along the direction of vibration, whether or not gravity is involved. Thus, we expect that this phenomenon also mitigates the effect of jet-driven streaming due to imperfect flow straightening and the effect of Rayleigh streaming, on Earth in zero gravity, because both of these streaming phenomena create non-axial density gradients in pulse tubes.¹² However, since streaming grows more intense as ωa rises, the mitigation cannot be as abrupt a function of ωa as it is for gravity-driven convection. Nevertheless, at a given ΔT , the effect of streaming might be reduced significantly.

The rest of this section presents a very simple attempt to anticipate the best choice for l in Eq. (20) when the pulse-tube's length L is significantly greater than its diameter D , which is a common situation in pulse-tube refrigerators. Although the approximations used here might seem crude, we hope that they can correctly capture the dominant functional dependences on D and L .

Three characteristic times are well separated. For a typical sinusoidally driven pulse-tube refrigerator, $1/\omega \sim 0.003$ s. This is significantly faster than the time required for an appreciable change in convective motion, estimated from the ring-pendulum analysis to be of the order of $\sqrt{l/g} \sim 0.1$ s. This, in turn, is significantly faster than the diffusive thermal-relaxation time $l^2/\kappa \sim 30$ s. Thus, for rough estimates, it is plausible to assume that temperatures are essentially carried with the moving gas on the time scales of the gas motion and that the dynamical behavior of the gravity-vibration interaction in the gas is qualitatively similar to that of the ring pendulum.

Furthermore, since $\nu \sim \kappa$ in gases, the viscous relaxation time for l -scale distance is also ~ 30 s, so the viscous penetration depth $\sqrt{2\nu/\omega}$ is typically much smaller than l . The velocity of the developing steady flow might be of the order of $l/\sqrt{l/g}$, so the steady-flow Reynolds number might ini-

tially be roughly $(l^2/\nu)/\sqrt{l/g} \sim 300$, a regime in which inertial effects are important and two- and three-dimensional flows are often time dependent. The typical Rayleigh number given in Eq. (18) can be estimated as $(l^2/\nu)(l^2/\kappa) \times (\Delta T_{\text{char}}/T_{\text{char}})/(l/g) \sim 10^6 \Delta T_{\text{char}}/T_{\text{char}}$, so modest $\Delta T_{\text{char}}/T_{\text{char}}$ can cause significant convection. Similarly, the typical vibrational Rayleigh number in Eq. (19) can be estimated as $10^8 (a/l)^2 (\Delta T_{\text{char}}/T_{\text{char}})^2$, so values of a/l that are common in pulse tubes can make $\text{Ra}_{\text{vib}} \sim \text{Ra}$.

To keep the analysis of the problem simple, we retain the Boussinesq approximation, treating the gas in the pulse tube as incompressible. Thus, the double-headed arrows in Fig. 1(d), illustrating the peak-to-peak stroke of the gas, are taken to be the same length at the two ends of the pulse tube. The isotherms in Fig. 1(d) are shown at an instant of time when the motion of the gas is at mid-stroke, e.g., when $\omega t = -\pi/2$. A quarter cycle later, $\cos \omega t = 1$ and the uppermost isotherm would have just touched the cold heat exchanger; another half cycle later, when $\cos \omega t = -1$, the lowermost isotherm would just touch the hot heat exchanger. The slug of gas between these two isotherms, which always remains inside the pulse tube, is the object of interest. It has a length $L - 2a$, which we might take to be the effective length for this problem. However, our experiments cannot resolve the small difference between this length and L itself, so for simplicity we use L in the rest of this derivation.

The uppermost isotherm has temperature T_C when it is momentarily in contact with the cold heat exchanger at that temperature, but the pressure-induced adiabatic heating and cooling that the gas experiences causes its average temperature to be $T_{C,\text{avg}} = T_C [1 + (\gamma - 1) p_a \sin \beta / \gamma p_m]$, where γ is the ratio of isobaric to isochoric specific heats, p_a is the pressure amplitude, p_m is the mean pressure, and $\beta = \pi/2$ is the phase by which oscillating pressure leads oscillating velocity (positive velocity going from hot to cold).¹³ The hot isotherm's temperature $T_{H,\text{avg}}$ obeys a similar expression. Our experiments cannot resolve the effects of these small p_a -dependent temperature differences, so for simplicity we describe the temperatures of the slug of gas with $\Delta T = T_H - T_C$ and $T_{\text{avg}} = (T_H + T_C)/2$ in the rest of this derivation, instead of similar but more complicated expressions with $T_{H,\text{avg}}$ and $T_{C,\text{avg}}$.

As shown in Fig. 2(a), imagine that motion within this slug of gas in the pulse tube can be modeled as plug flow in a loop of piping that vibrates along the θ direction and whose cross-sectional area is half of the cross-sectional area A of the pulse tube itself, so gas rising on the left half of the pulse tube in Fig. 1(d) is modeled as rising plug flow in the left leg of Fig. 2(a), and similarly down on the right. In this model, the convective motion in the pulse tube is represented by a single degree of freedom, measured by a time-dependent displacement $\delta(t)$. This displacement and the superimposed vibration carry the isotherms, because the thermal-relaxation time is so much slower than the times for these motions, as estimated above. Then 2δ is the measure of how far the isotherms in the right half of the loop are misaligned from those in the left half at any instant of time, with the sign of δ as shown in the figure. Ignoring end effects for small δ , and assuming that end-to-end temperature differences are small enough that the density ρ can be assumed to be essentially

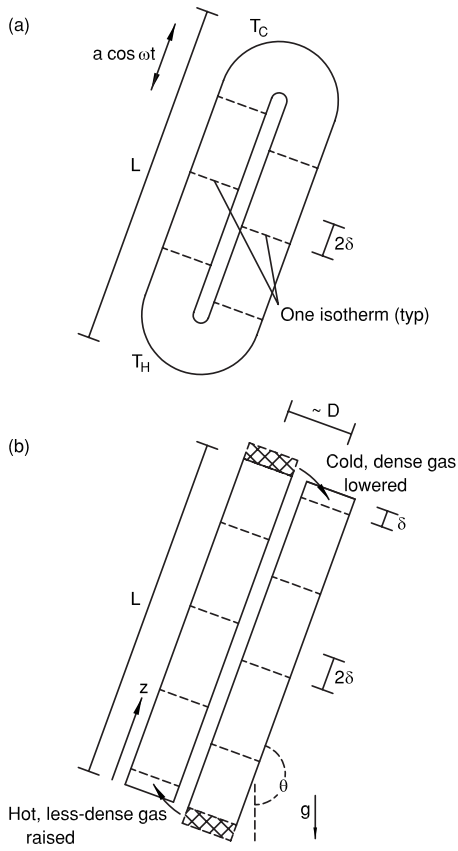


FIG. 2. (a) The convective flow in the pulse tube can be modeled crudely as plug flow in a loop of pipe, characterized by a single degree of freedom, measured by δ . As shown, the plug-flow displacement δ creates a misalignment of 2δ between isotherms on the left and right legs of the loop. A change in δ can be caused by gravity, or by the vibration acting on an off-center center of mass caused by nonzero δ itself. (b) The effect of a change in δ on the gravitational potential energy of the gas in such a loop of pipe can be estimated from an even more simplified model.

linear in position [not obviously a good assumption, but linear $T(z)$ is discussed below], the density in the two legs of the loop can be written as

$$\rho(z) = \rho_H + (z \pm \delta)\Delta\rho/L \quad (21)$$

except near the ends, where z is the distance from the hot end, $\Delta\rho = \rho_C - \rho_H$, the plus sign is chosen for the right leg and the minus sign for the left leg, and the subscripts on ρ correspond to those on T above. Thus, when $\delta = 0$, the density rises linearly from ρ_H at $z = 0$ to ρ_C at $z = L$ in both legs, and nonzero δ shifts one of these density profiles up and the other one down.

A Lagrangian derivation of the equation of motion for $\delta(t)$ is well suited to keeping track of details here. The applied vibrational displacement $a \cos \omega t$ is superimposed on the plug-flow displacement δ , so the velocity of the gas is $-\omega a \sin \omega t + \dot{\delta}$ in the left leg of the loop and $-\omega a \sin \omega t - \dot{\delta}$ in the right leg. Transverse kinetic energy near the ends, and other end corrections to the kinetic energy, are neglected because $D \ll L$ is assumed. Then the total kinetic energy is

$$K = \frac{1}{2}(\rho_{\text{avg}} - \Delta\rho\delta/L)\frac{A}{2}L(-\omega a \sin \omega t + \dot{\delta})^2 + \frac{1}{2}(\rho_{\text{avg}} + \Delta\rho\delta/L)\frac{A}{2}L(-\omega a \sin \omega t - \dot{\delta})^2 \quad (22)$$

$$= \frac{AL}{2}\rho_{\text{avg}}(\omega^2 a^2 \sin^2 \omega t + \dot{\delta}^2) + A\Delta\rho\delta\dot{\delta}\omega a \sin \omega t. \quad (23)$$

In Eq. (22), the first term is the kinetic energy in the left leg of the loop, and the second term that in the right leg. The density factors in these terms come from averaging Eq. (21) with respect to z .

The potential energy change U due to δ can be estimated by considering Fig. 2(b). As δ changes from zero to a nonzero value, isotherms far from the ends of the tube contribute no change to U , because for any mass moving up in the left leg there is an equal mass associated with the same isotherm moving down the same distance in the right leg. The same cancellation would occur for the gas within δ of the end of the tube, if it did not have to “turn the corner,” changing from the left leg to the right leg at the top or the right to the left at the bottom; if such gas parcels could move to the positions shown as crosshatched in Fig. 2(b), their effects on U would be canceled by their partners of the same isotherms in the other leg. Thus, the net effect of nonzero δ is to lower some cold gas whose mass is of the order of $\rho_C(A/2)\delta$ a distance of the order of $D \sin \theta - \delta \cos \theta$ and raise some hot gas whose mass is of the order of $\rho_H(A/2)\delta$ a similar distance, yielding

$$U \simeq -\Delta\rho\frac{A\delta}{2}g\left(\frac{4}{3\pi}D \sin \theta - \delta \cos \theta\right), \quad (24)$$

where the $4/3\pi$ comes from careful consideration of the semicircular cross section of each leg.

With the standard Lagrangian methods of classical mechanics, the equation of motion for δ is obtained by writing $(d/dt)\partial[K-U]/\partial\dot{\delta} - \partial[K-U]/\partial\delta = 0$. Using Eqs. (23) and (24) above for K and U , the result is

$$\rho_{\text{avg}}AL\ddot{\delta} = \frac{A\Delta\rho g}{2}\left(\frac{4}{3\pi}D \sin \theta - 2\delta \cos \theta\right) - A\Delta\rho\omega^2 a \delta \cos \omega t. \quad (25)$$

This equation resembles Eq. (7) for the unbalanced-ring pendulum. The total mass $\rho_{\text{avg}}AL$ in the loop of piping accelerates in the δ direction in response to forces of gravity, expressed by the first term, and in response to forces caused by vibration, expressed by the second term. Following the same procedure as for the unbalanced-ring pendulum, this equation of motion is broken down into fast and slow parts by substituting $\delta = \delta_{\text{slow}} + \delta_{\text{fast}} \cos \omega t$ and assuming $\delta_{\text{fast}} \ll \delta_{\text{slow}}$ and $\omega^2 \gg \Delta\rho g / \rho_{\text{avg}}L$. The fast part of δ is then

$$\delta_{\text{fast}} = \frac{\Delta\rho}{\rho_{\text{avg}}}\frac{a}{L}\delta_{\text{slow}}, \quad (26)$$

and the slow response of δ to gravity and to the time-averaged product of δ_{fast} and the imposed vibration is described by

$$\rho_{\text{avg}}AL\ddot{\delta}_{\text{slow}} = \frac{A\Delta\rho g}{2} \left(\frac{4}{3\pi}D \sin \theta - 2\delta_{\text{slow}} \cos \theta \right) - \frac{A(\Delta\rho)^2\omega^2a^2\delta_{\text{slow}}}{2\rho_{\text{avg}}L}. \quad (27)$$

If the vibrations suppress convection, then $\ddot{\delta}_{\text{slow}}=0$, and the phenomenon should be governed by the surviving terms on the right-hand side. Solving for δ_{slow} yields

$$\delta_{\text{slow}} = \frac{4D \sin \theta/3\pi}{\omega^2a^2\Delta\rho/\rho_{\text{avg}}gL + 2 \cos \theta}. \quad (28)$$

Too large a value of δ_{slow} would be unrealistic, because it would put the off-center cold gas and the off-center hot gas in Figs. 1(d) and 2(b) close together, thermally short-circuiting the temperature difference responsible for the vibration-stabilization effect. Thus, a stable δ_{slow} can be no larger than some fraction of L , which can be conveniently written as $2L/3\pi\alpha$, where α is as yet unknown. Making that substitution for δ_{slow} in Eq. (28), rearranging, and defining a dimensionless group of variables resembling Eq. (14) yield

$$N_{\text{pic}} \equiv \frac{\omega^2a^2}{g(\alpha D \sin \theta - L \cos \theta)} \frac{\Delta\rho}{\rho_{\text{avg}}} = 2. \quad (29)$$

Since $\Delta\rho/\rho_{\text{avg}}=\Delta T/T_{\text{avg}}$, this supports the dependences shown in Eq. (14) above, for $\beta=1$. Note that this derivation is valid for $90^\circ \leq \theta \leq 180^\circ$, so the geometrical factor in the denominator could just as well be written as $\alpha D|\sin \theta| + L|\cos \theta|$.

Equations (28) and (29) are only valid for ωa large enough to suppress convective motion. For very large ωa , δ_{slow} is generally small, as illustrated in Fig. 2(b). However, if ωa is just below the threshold, δ_{slow} could be fairly large and essentially time dependent, and the picture of Fig. 2(b) would be unrealistic because the off-center slugs of extreme-temperature gas would extend over appreciable lengths, and their temperatures would no longer be uniformly at T_C and T_H , but rather would be distributions of less-extreme temperatures determined by competing conduction to both heat exchangers and between the two legs of the loop. Whether this might lead to $N_{\text{pic}} \sim (\Delta T/T_{\text{avg}})^\beta$, where $\beta < 1$, is not clear. Further analysis of this issue may require numerical study of Eqs. (15)–(17) and other information in Ref. 11.

Repeating this section's analysis but starting with the assumption that $1/\rho \propto T$ is linear in z instead of the assumption of Eq. (21) that ρ is linear in z leads tediously to

$$\frac{(\Delta T)^2}{T_C T_H \ln(T_H/T_C)} \quad (30)$$

instead of $\Delta\rho/\rho_{\text{avg}}$ in Eq. (29). The difference between $\Delta T/T_{\text{avg}}$ and Eq. (30) is only $(\Delta T)^3/2T_{\text{avg}}^3$ to lowest order in $\Delta T/T_{\text{avg}}$. The accuracy of the measurements described below does not justify the extra complexity of Eq. (30), so we retain the simpler $\Delta T/T_{\text{avg}}$ and $\Delta\rho/\rho_{\text{avg}}$ dependences in Eqs. (14) and (29).

The high-amplitude stability of pulse tubes against gravity-driven convection was characterized by Wang and Gifford⁸ in terms of the inverse of the dimensionless group

$$\frac{u_a^2}{gD\Delta T/T_{\text{avg}}} = \frac{\omega^2a^2T_{\text{avg}}}{gD\Delta T}, \quad (31)$$

which is similar to Eqs. (29) and (14), but with two important differences. First, the choice of Ref. 8 keeps g and ΔT together in the denominator, while our derivation of Eq. (29) shows that the nonlinear nature of the stabilizing effect of vibrations puts $(\Delta\rho)^2$ in the last term in Eq. (27) and, hence, puts $\Delta\rho$ in the numerator of Eq. (29), leaving g in the denominator: In contrast to the dependence shown in Eq. (31), higher temperature differences actually allow suppression of convection at *lower* frequencies and amplitudes, even while a larger acceleration of gravity would require higher amplitudes. Second, Ref. 8 arbitrarily chose D as the characteristic length in the dimensionless group, while our derivation shows that the characteristic length might best be considered to be θ dependent, and that L is more important than D when $D \ll L$, except very close to $\theta=90^\circ$.

III. EXPERIMENTS

To investigate these phenomena under a broad range of experimental conditions, an apparatus with interchangeable tubes much simpler than complete pulse-tube refrigerators was built. Working only at and above ambient temperature allowed the use of easily measured electric-resistance heat, without refrigeration, and adoption of nearly standing-wave phasing for the measurements eliminated need for a pulse-tube refrigerator's orifice and compliance tank, simplified the apparatus, reduced surface areas that could contribute to room heat leaks, reduced the heat demands on the heat exchangers, and led to rapid thermal-equilibration times. Five tubes, shown to scale in Fig. 3 and described in Table I, were used for these measurements.

Each of the five pulse tubes (or thermal-buffer tubes) was a right-circular cylindrical space bounded around its sides by a 0.8-mm-thick stainless-steel wall and on its ends by diffusion-bonded stainless-steel screens acting as flow straighteners. Each flow straightener comprised 27 layers of nominally 16.5 wires/cm, 0.14-mm-diameter-wire square-weave screen, with alternate layers turned 45° . They were cut to a diameter that was 1.6 mm greater than that of each pulse-tube's inside diameter, by wire electric-discharge machining after diffusion bonding, so steps on the ends of the pulse tube could hold them firmly in place and define the pulse-tube length L accurately. Beyond these flow straighteners were drilled copper disks that served as heat exchangers, maintaining nearly isothermal planes across the ends of the flow straighteners by conducting heat to or from their surroundings. The heat-exchanger holes were 1.32 mm in diameter, and the hole patterns were designed for spatially uniform coverage over the pulse-tube area.

On the hot end, a bounce space the same diameter as the pulse tube allowed significant oscillating flow through the hot heat exchanger, and a 1.5-mm-diameter sheathed type- K thermocouple in that space, a few millimeters from the hot heat exchanger, measured T_H . The thermocouple was bent, as shown in the figure, so almost 1 cm of its tip lay close to the heat exchanger (except for the thinnest tube, in which the

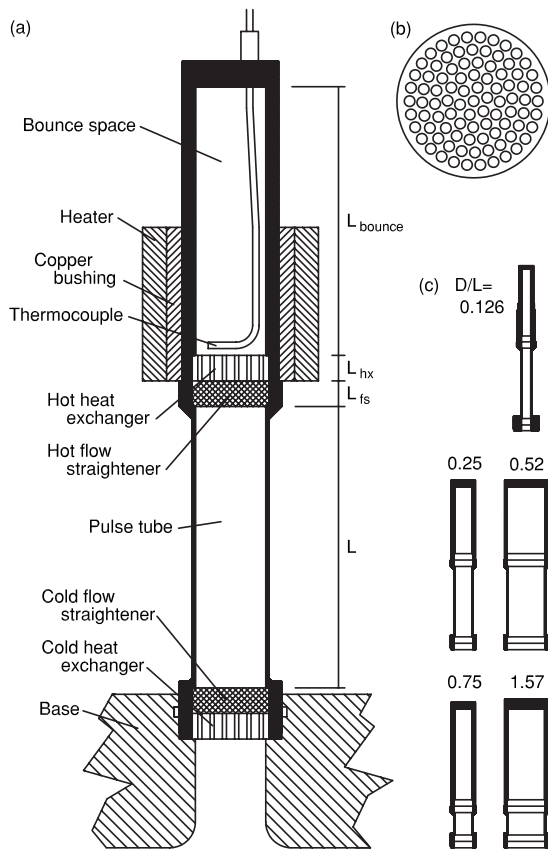


FIG. 3. (a) Cross-sectional scale drawing of the $D/L=0.25$ tube, shown with the cold end down (i.e., $\theta=0$). The dimensions L_j are given in Table I. The pressure-vessel boundary, shown in heavy black, was a long, machined tube with a cap welded into one end. The cap pressed on a thin-walled sleeve in the bounce space (not distinct in the figure), whose inside diameter was the same as that of the pulse tube, thereby trapping the hot heat exchanger and hot flow straightener against a machined step at the top of the pulse tube. The cap included a welded-in compression fitting through which the hot thermocouple passed. Clamps holding the tube to the base are not shown. (b) A perpendicular cross section through one of the drilled copper heat exchangers, at twice the scale of (a). (c) The proportions of all five tubes, at 1/4 the scale of (a).

bent portion was necessarily shorter). A commercial “band” electric-resistance heater provided heat, that heat being spread around the hot heat-exchanger region by a copper bushing. Ceramic-fiber thermal insulation covered all the hot parts including the pulse tube itself. The cold end was mounted in a water-cooled aluminum base, whose temperature T_C varied no more than 1°C during the course of any single data set, and did not differ from 20°C by more than a few degrees from week to week.

A passage through the aluminum base, a few centimeters long, led from the cold heat exchanger to the top of a 10-cm-diameter piston, which was driven by a linear motor¹⁴ to whose housing the aluminum base was bolted. The motor was best operated very near the resonance frequency defined by its large moving mass and the gas-pressure spring constant experienced by the piston. This resonance frequency was easily varied by adjusting the mean pressure, and could be changed for a desired mean pressure by inserting volume-adding spacer rings between the motor housing and the aluminum base. The motor housing was mounted on a modified rotary stand, originally intended for rebuilding automobile engines. The rotary part of the stand had a hole-and-pin mechanism for reproducibly setting the tilt of the entire apparatus in 10.0° increments from 0.0° to 180.0° . A bubble level was used to align the pulse tube with gravity to $<0.1^\circ$ with the apparatus set at 180.0° . The pressure amplitude p_a applied at the bottom of the pulse-tube assembly was measured with a lock-in amplifier connected to a piezoresistive transducer¹⁵ in the aluminum base.

In the $D/L=0.52$ tube, a second thermocouple was installed, in the copper bushing under the electric-resistance heater. Near $T_H=250^\circ\text{C}$, the bushing thermocouple was never more than 10°C hotter than the internal thermocouple, this temperature difference being largest when the convective heat transport was the largest.

TABLE I. Dimensions for the five tubes used in the experiments, and the heat \dot{Q}_{gascon} carried by simple conduction in the gas in each tube under typical experimental circumstances. See also Fig. 3(c) for scale drawings.

$D/L=$	0.126	0.249	0.521	0.750	1.57
	Dimensions				
D (cm)	0.88	1.74	3.64	1.74	3.64
L (cm)	6.98	6.99	6.99	2.32	2.32
L_{fs} (cm)	0.64	0.64	0.64	0.64	0.64
φ_{fs}	0.82	0.82	0.82	0.82	0.82
L_{hx} (cm)	0.56	0.56	0.56	0.56	0.56
No. of hx holes	19	91	331	91	331
φ_{hx}	0.427	0.521	0.436	0.521	0.436
Holes' R_{hx} (mm)	0.66	0.66	0.66	0.66	0.66
L_{bounce} (cm)	6.66	6.74	6.74	9.02	9.02
	\dot{Q}_{gascon} (W)				
He, $T_H=425^\circ\text{C}$		0.30			
He, $T_H=250^\circ\text{C}$	0.038	0.148	0.65	0.45	1.96
He, $T_H=150^\circ\text{C}$		0.076			
0.9He–0.1Ar, $T_H=250^\circ\text{C}$		0.121			
Ar, $T_H=250^\circ\text{C}$		0.019			

Obtaining one set of data typically took half of a day. A gas, its mean pressure p_m , a frequency, and a tip angle θ were chosen, and were kept fixed for each data set. An initial motor drive voltage was chosen, and heat was applied to the electric-resistance heater to maintain the hot temperature at a selected T_H . To assess that process, temperature was displayed as a function of time with a chart recorder. The heater voltage was adjusted manually until a steady setting achieved both a low rate of change in temperature (less than 0.1°C in a few minutes) and the desired T_H . The steady-state heater voltage V and pressure amplitude p_a were then recorded, and the heater power \dot{Q} was obtained by squaring the voltage and dividing the result by the heater's resistance. The motor drive voltage was changed to a new value, and the heat adjustment and data recording were repeated, typically at rates of two to four data points per hour.

Figure 4(a) shows six such data sets, all in the $D/L = 0.25$ tube with 3.1-MPa helium gas driven at 100 Hz, and with $T_C = 20^\circ\text{C}$ and $T_H = 250^\circ\text{C}$.

At $\theta = 0^\circ$, the cold end of the pulse tube was straight down so the gas was convectively stable. The measurements show that 14 W of heat were needed to keep $T_H = 250^\circ\text{C}$ in this tube, with amplitude-dependent variation being only a fraction of 1 W. Calculations show that the helium in the pulse tube conducted 0.15 W and the stainless-steel pulse-tube wall conducted 2.5 W, so most of the required heat was apparently heat leak through the fiber insulation to the room. Calculations¹⁶ that include boundary-layer heat shuttle along the pulse tube and acoustic-power dissipation in the hot heat exchanger and flow straightener show that the required heat should drop quadratically by 0.8 W as the oscillation amplitude rises from $p_a/p_m = 0.01$ to $p_a/p_m = 0.05$, in rough agreement with the $\theta = 0^\circ$ measurements.

Compared with $\theta = 0^\circ$, only a little more heat was convected at $\theta = 60^\circ$ at zero or low oscillation amplitude. This tube was slender enough that the highest edge of its cold end was still 1.0 cm below the lowest edge of its hot end at $\theta = 60^\circ$, so the gas in the tube can still be regarded as convectively stable at this tip angle.

At $\theta = 90^\circ, 120^\circ, 150^\circ$, and 180° over 4 W of heat was convected through the tube when no oscillations were present, representing Nusselt numbers ranging from 30 at 90° to 50 at 150° . Such convection is large enough to reduce the cooling power of a pulse-tube refrigerator significantly. The Rayleigh number based on L is about 27×10^6 , and such Nusselt numbers are plausible at this Rayleigh number: Eq. (4.89) in Ref. 17 yields a Nusselt number of 18 under these conditions, for $\theta = 180^\circ$. (However, our enclosure has porous ends, which could tend to increase the Nusselt number.) From the convective heat flow, ρ , c_p , and ΔT , we estimate that the convective velocity was of the order of 1 cm/s, roughly 100 times less than the typical oscillating velocity. The Reynolds number of the convective motion here is of the order of 20, so the convection should be laminar. This suggests that numerical calculations based on Ref. 11 may yield reliable results in this range of parameter space. However, in the tubes with $D/L \geq 0.5$ we did sometimes see time-dependent convection, evidenced by time dependence in the hot temperature, whose variations were as high as a few

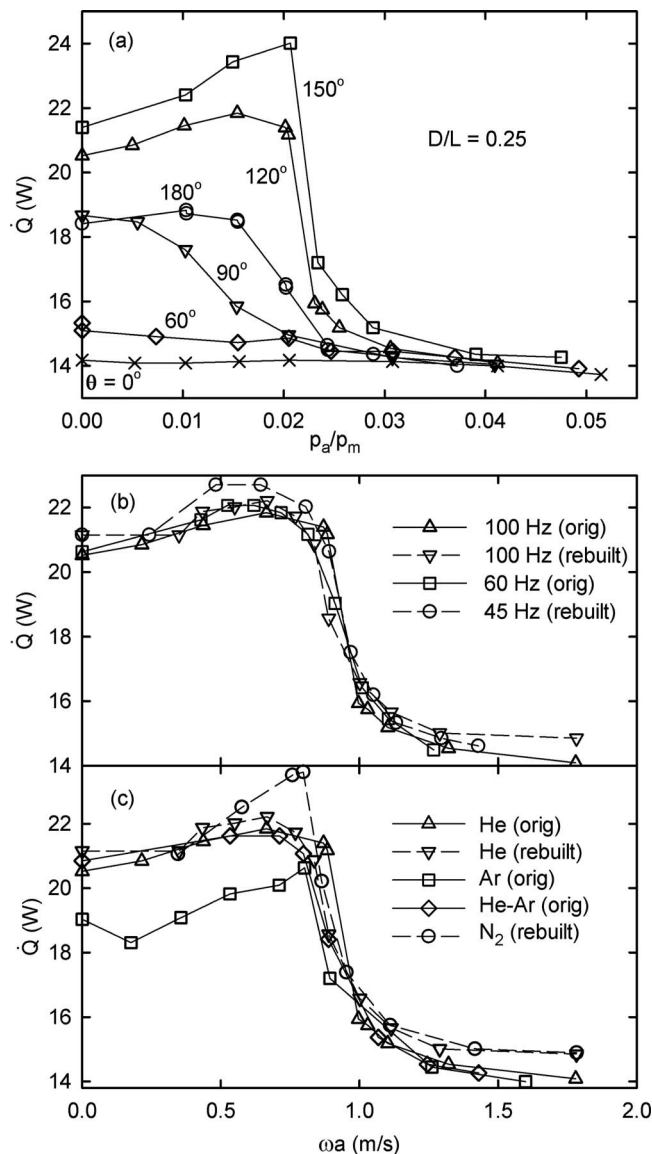


FIG. 4. Heat \dot{Q} required to maintain a steady hot temperature under a wide variety of conditions with 3.1-MPa gas in the $D/L = 0.25$ tube. The points are measurements, and the lines are only guides to the eyes. (a) Heat required to maintain $T_H = 250^\circ\text{C}$, with helium at 100 Hz, for six tip angles θ . The horizontal axis is the pressure amplitude at the base, divided by mean pressure. (b) Heat required to maintain $T_H = 250^\circ\text{C}$, with helium at $\theta = 120^\circ$, for three frequencies. (c) Heat required to maintain $T_H = 250^\circ\text{C}$, at 100 Hz, at $\theta = 120^\circ$, for four different gases. The mixture was 90% helium and 10% argon. The horizontal axis in (b) and (c) is the square root of the relevant part of Eq. (14), because this keeps the points almost equally spaced, making the variations near the transition easier to see.

tenths of a degree over time scales of about 10 s. The time dependence started near the convection-suppression transition and rose with amplitude, and was greatest for the tube with the highest D/L . Numerical calculations in the time-dependent regime might be more challenging.

Figure 4(a) shows an initial rise in convective heat transfer with amplitude for $\theta \geq 120^\circ$. Possible explanations for this phenomenon include a weakening of the zero-velocity boundary condition at the ends of the convective cell as those ends find themselves, on average, farther from the flow straighteners at higher amplitude, and a strengthening of thermal contact near the ends of the convective cell as jets

whose diameters are of the order of the flow-straighteners' hydraulic radius squirt gas at the heat-exchangers' temperatures into the ends of the convective cell.

Figure 4(a) also shows that the convection was effectively stopped when the oscillations had a high enough amplitude, as expected from Secs. I and II.

The closely spaced points near the 120° transition and the essentially overlapping points throughout the 180° data indicate attempts to observe hysteresis, by taking some of the data while systematically increasing p_a and other data while systematically decreasing p_a . No hysteresis was observed in these data sets or in any others. [A near exception is described in the caption for Fig. 6(b).]

To plot such data as a function of ωa or of N_{ptc} , we converted from the measured p_a/p_m to the vibration amplitude a in the middle of the pulse tube by using

$$a = \frac{p_a}{\gamma p_m} \left(\frac{L}{2} + \gamma \varphi_{f_s} L_{f_s} + \left[1 + (\gamma - 1) \frac{\delta_\kappa}{R_{hx}} \right] \varphi_{hx} L_{hx} + L_{\text{bounce}} \right), \quad (32)$$

where half of the pulse-tube length, $L/2$, the hot-flow-straightener length L_{f_s} , the hot-heat-exchanger length L_{hx} , and the bounce-space length L_{bounce} add up to the total distance between the middle of the pulse tube and the closed end of the experiment. This expression is based on the assumptions that p_a is independent of x from the middle of the pulse tube to the end of the bounce space, and that thermal-hysteresis effects in the bounce space and pulse tube are negligible. Thus, if the total distance were unobstructed and of uniform cross-sectional area, then Eq. (32) would be simply $a = (p_a/\gamma p_m)(L/2 + L_{f_s} + L_{hx} + L_{\text{bounce}})$, describing simple adiabatic compressions and expansions everywhere. The prefactor $p_a/\gamma p_m$ is used in Eq. (32) because most of that length, $L/2 + L_{\text{bounce}}$, does experience nearly adiabatic compressions and expansions. The prefactors of the small L_{f_s} and L_{hx} terms in Eq. (32) account for the volumetric porosities φ_j of those components, the isothermal nature of the oscillations in the flow straightener, and the thermal hysteresis in the circular channels through the heat exchanger, in which the channel radius is R_{hx} and the thermal penetration depth is δ_κ . Numerical estimates¹⁶ that include inertial and resistive pressure drops in the hot heat exchanger and flow straightener and the consequences of thermal hysteresis elsewhere suggest that these assumptions introduce errors of no more than 2% to the determination of a .

Figure 4(b) shows convection-suppression data from the $D/L=0.25$ tube at three different frequencies, all with 3.1-MPa helium at $\theta=120^\circ$ and $T_H=250^\circ\text{C}$. Although the frequency ranges over a factor of 2, plotting these data sets as functions of ωa aligns them very well, corroborating the ωa functional dependence on N_{ptc} in Eq. (14), and contradicting any other supposed strong dependences on ω or a in this tube, such as a/L (independent of ω) or $\omega a^2/L$.

[The “100 Hz (orig)” data set in Fig. 4(b) is also shown in Fig. 4(a). After taking that data set and the “60 Hz (orig)” set, the original $D/L=0.25$ tube was disassembled to use parts elsewhere, and later was “rebuilt” to obtain more data. The difference between the “original” and “rebuilt” 100-Hz

sets is presumably due to slight hardware irreproducibility, including slightly different hot-thermocouple positions. For future work, we recommend a reproducible attachment of both thermocouples directly to their copper heat exchangers.]

Figure 4(c) shows convection-suppression data from the $D/L=0.25$ tube for four different gases at 3.1 MPa and 100 Hz, with $T_H=250^\circ\text{C}$ and $\theta=120^\circ$. The horizontal alignment of all of these data sets confirms the lack of explicit gas-property dependence of N_{ptc} . The alignment of the helium and argon data, despite the tenfold difference in atomic mass and mass density, confirms that N_{ptc} should be independent of molecular mass. The alignment of the helium-argon data with the pure-monatomic-gas data, despite the mixture's 32% lower Prandtl number, confirms that N_{ptc} is independent of Prandtl number and, by inference, independent of the gas transport properties. The alignment of the $\gamma=7/5$ nitrogen data with the $\gamma=5/3$ monatomic-gas data confirms that N_{ptc} is independent of the specific-heat ratio, except through the conversion from p_a/p_m to a given in Eq. (32).

To investigate the ΔT dependence of the convection-suppression transition, we used the $D/L=0.25$ tube with 3.1-MPa helium and $\theta=120^\circ$ at 100 Hz, at three different hot temperatures. To bring the data into approximate *vertical* alignment, we divided \dot{Q} by ΔT , and then subtracted 0.08, 0.06, and 0.05 W/ $^\circ\text{C}$ from the 425, 250, and 150 $^\circ\text{C}$ data, respectively, to account for the temperature-dependent heat leaks. With the three data sets plotted against ωa in Fig. 5(a), it is apparent that it was easier to suppress the convection at higher ΔT . Figures 5(b) and 5(c) show these three data sets plotted against $\omega a \sqrt[4]{\Delta T/T_{\text{avg}}}$ and $\omega a \sqrt{\Delta T/T_{\text{avg}}}$. The data align best using the fourth root, which is why we choose $\beta=1/2$ in Eq. (14), despite the fact that the derivation of Sec. II yields $\beta=1$.

To study the L and D dependence of the convection-suppression transition, we used data from all five pulse tubes, which had five different aspect ratios. Measurements with identical gas, temperatures, and frequency are shown in Figs. 4(a) and 6. Like the $D/L=0.25$ tube, which yielded the data shown in Figs. 4 and 5, the $D/L=0.52$ tube displayed sharp convection-suppression transitions at $\theta=120^\circ$ and 150° , and a $\theta=0$ heat requirement that was almost independent of amplitude, as shown in Fig. 6(b). In the $D/L=0.75$ tube, the transitions were still sharp, but the $\theta=0$ heat requirement rose dramatically, and quadratically, with amplitude, as shown in Fig. 6(c). The $D/L=1.57$ tube showed a similar rising baseline heat requirement, but a very ill-defined and incomplete transition to reduced convection, as shown in Fig. 6(d). Our motor did not let us learn whether higher amplitudes would bring a second, more complete reduction in convection in this tube. Unlike the other four tubes, the $D/L=0.126$ tube did not have sharp transitions at any tip angle, as shown in Fig. 6(a), and the small heats involved were difficult to measure accurately.

We do not understand some of these qualitative differences between the data sets in the different tubes. The quadratically rising $\theta=0$ heats for the two shortest tubes suggest streaming, but the calculated Rayleigh streaming velocity¹⁸ just outside the boundary layer at mid-tube is very nearly the same, 1.3 cm/s at $p_a/p_m=0.025$, for all five tubes, and esti-

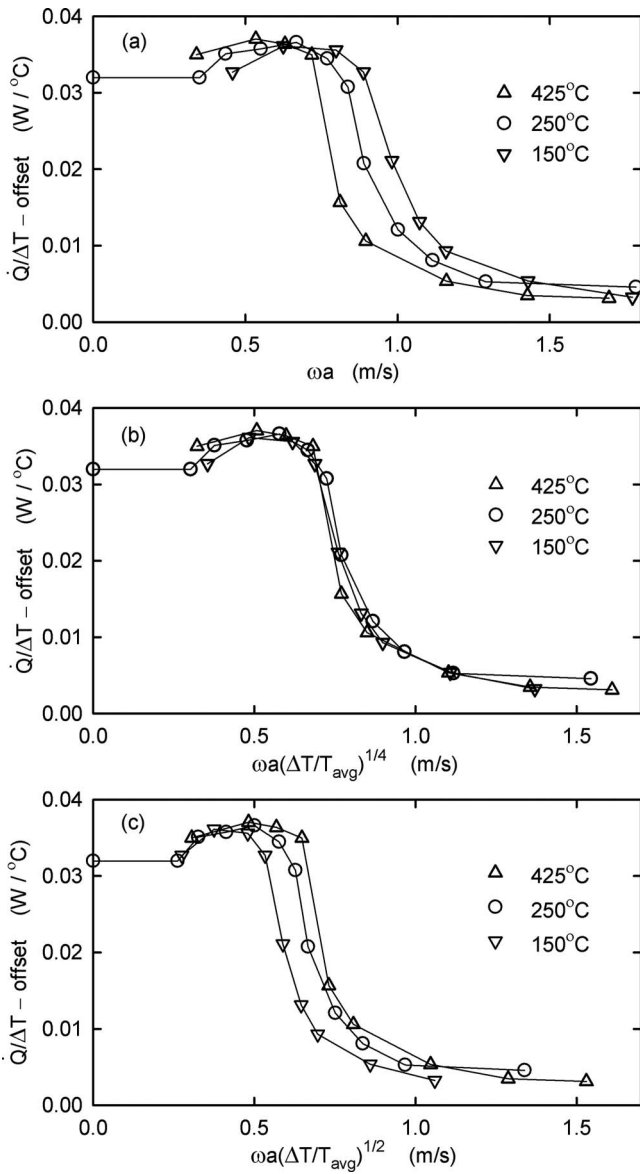


FIG. 5. Normalized heat required to maintain a steady hot temperature in the (rebuilt) $D/L=0.25$ tube, with 3.1-MPa helium and $\theta=120^\circ$, at three different hot temperatures T_H with which the points are labeled. (N.B.: ΔT is $\sim 20^\circ\text{C}$ smaller than T_H .) The points are measurements, and the lines are only guides to the eyes. The experimental temperature dependence is closer to the fourth root used in (b) than to either the square root used in (c) or no temperature dependence used in (a).

mates of the heat that such streaming can transport along the tubes¹⁹ range only from 0.1 to 0.5 W at that p_a/p_m , too small to explain the measurements. Seeking another reason that the short tubes differ from the long tubes, one can consider the stroke divided by the tube length, $2a/L$, which should be smaller than 1 to prevent gas from shuttling heat all the way from the hot flow straightener to the cold flow straightener every cycle of the oscillation. But $2a/L$ is only 0.12 at the $\theta=120^\circ$ transition in the $D/L=0.75$ tube, where the rising baseline is perhaps even visible as low as $2a/L \approx 0.07$, so shuttle heat should not be responsible for the rising baseline. Furthermore, the $D/L=0.25$ tube's 100-Hz, $\theta=0$ data reach as high as $2a/L=0.09$, and that tube's 45-Hz data extend to $2a/L=0.14$, with no suggestion of rising baselines in Figs. 4(a) or 4(b).

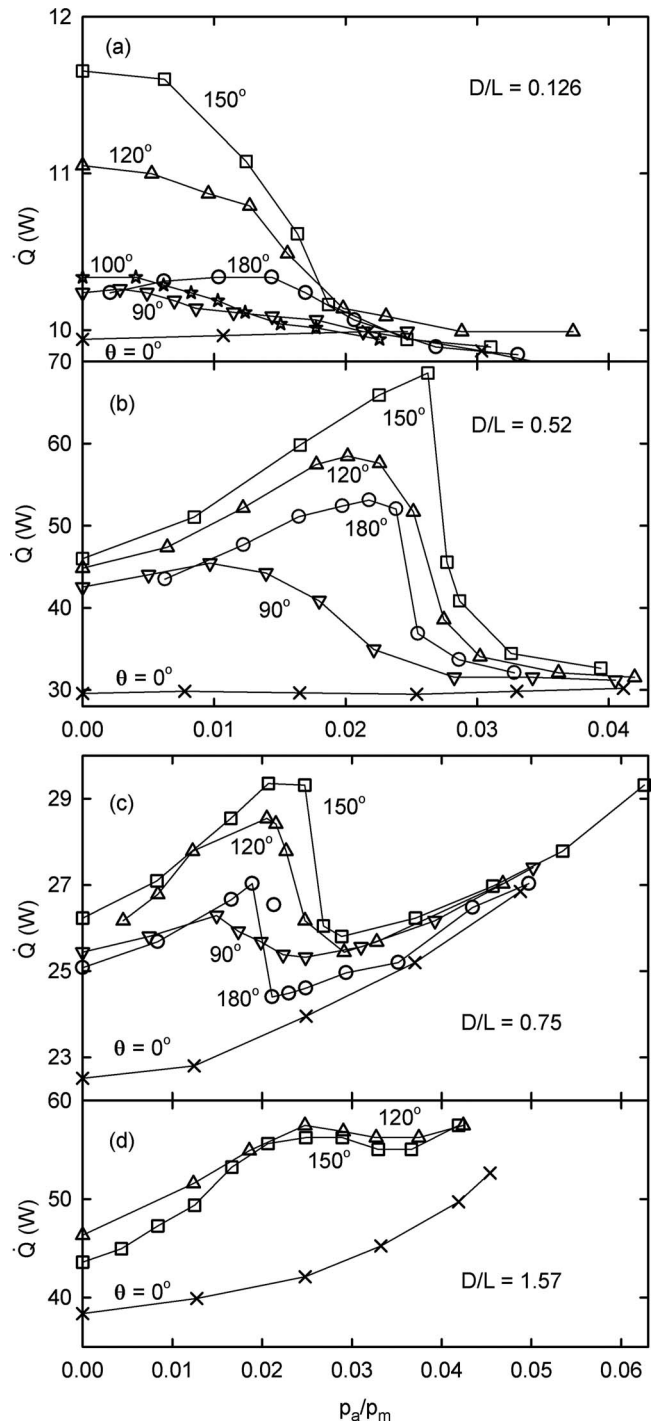


FIG. 6. Heat required to maintain $T_H=250^\circ\text{C}$ in 3.1-MPa helium at 100 Hz, in four different tubes. Figure 4(a) shows similar data for a fifth tube. The points are measurements, and the lines are only guides to the eyes. The horizontal axis is pressure amplitude at the base, divided by mean pressure. In (c), one of the 180° points is not connected with the lines. That data point was metastable: It persisted steadily for 5 min before the heat suddenly dropped to the point below it.

Despite this mystery, the data from the four tubes with the smallest D/L can be used to explore whether D or L is the most important geometrical variable l in Eq. (20) governing the convection-suppression transition, and to test the $aD \sin \theta - L \cos \theta$ geometry dependence given in Eq. (29) for small D/L . From each $\theta \neq 0$ data set in Figs. 4(a) and 5, we subtracted a quadratic fit to the corresponding $\theta=0$ base-

line data set, and defined the transition from convection to suppression as the value of p_a/p_m where each data set passes halfway between the maximum value of $\dot{Q}-\dot{Q}_{\text{baseline}}$ and zero. (This definition of the transition is essentially identical to the location of steepest decrease in $\dot{Q}-\dot{Q}_{\text{baseline}}$, except for the $D/L=1.57$ tube.) We converted the transition value of p_a/p_m to a corresponding transition value of a using Eq. (32).

Figure 7 displays the results as a function of D/L for three different choices of the characteristic length l that might be used in the dimensionless group in Eq. (20). First, Fig. 7(a) shows the results when plotted with $l=D$, the choice made in Ref. 8. For this choice of l , the transition displays complicated dependence on θ and D/L , suggesting that simply using $l=D$ in N_{ptc} does not provide a universal description of the transition. In fact, for $\theta=180^\circ$, the transition varies almost as $1/(D/L)$, as shown by the dashed curve, suggesting that dividing by D is a very poor choice for this particular θ . Next, in Fig. 7(b), the same data are plotted using $l=L$. Here, the $\theta \neq 90^\circ$ data collapse reasonably well along a single curve with little D/L dependence, but the $\theta=90^\circ$ data deviate significantly from the others; comparison to the dashed line shows that the $\theta=90^\circ$ transition varies almost as D/L for small D/L , suggesting that dividing by L is a poor choice for this particular θ . Finally, Fig. 7(c) shows the same data plotted using $l=\alpha D \sin \theta - L \cos \theta$, with $\alpha=1.5$. This choice brings the data sets for all tip angles close to a common curve, consistent with Eq. (29) in some ways. Trying $\alpha=1.0$, 2.5, or more-extreme values ruins the clustering of the data in Fig. 7(c), while using $\alpha=2.0$ looks only a little worse than $\alpha=1.5$. Using $\alpha=1.5$ sets $\delta_{\text{slow}}=2L/3\pi\alpha=0.14L$, which seems reasonable, being about three times larger than the δ_{slow} shown in Fig. 2.

IV. FURTHER DISCUSSION

The vibrational stabilization of an inverted pendulum is a useful guide to intuition about how acoustic oscillations suppress natural convection in an inverted pulse tube, and the dimensionless pulse-tube convection number N_{ptc} defined in Eq. (14) may provide a good quantitative framework for analysis, at least for small aspect ratios. Experiments confirm that ωa captures the relevant dependences on frequency and displacement, and that gas properties such as γ and Prandtl number are not important. However, the picture is incomplete, at best.

For example, the observed $\beta=1/2$ temperature dependence in Fig. 5 differs significantly from the $\beta=1$ prediction of Eq. (29). This remains a mystery. In the same figure, dividing \dot{Q} by ΔT brought the data into good vertical alignment, implying that the Nusselt number is independent of ΔT , while Eq. (4.89) in Ref. 17 predicts that the Nusselt number should be proportional to $(\Delta T)^{1/3}$.

Furthermore, we are not sure how to interpret the D/L dependence that remains in Figs. 7(c) and 7(d). One possibility is that the transition occurs at $N_{\text{ptc}} \approx 1$ for a substantial range of D/L , including $0.25 \leq D/L \leq 0.52$, as predicted for low D/L by Eq. (14) and suggested by the dashed line in Fig. 7(c). The data at $D/L=0.126$ might fall below this value

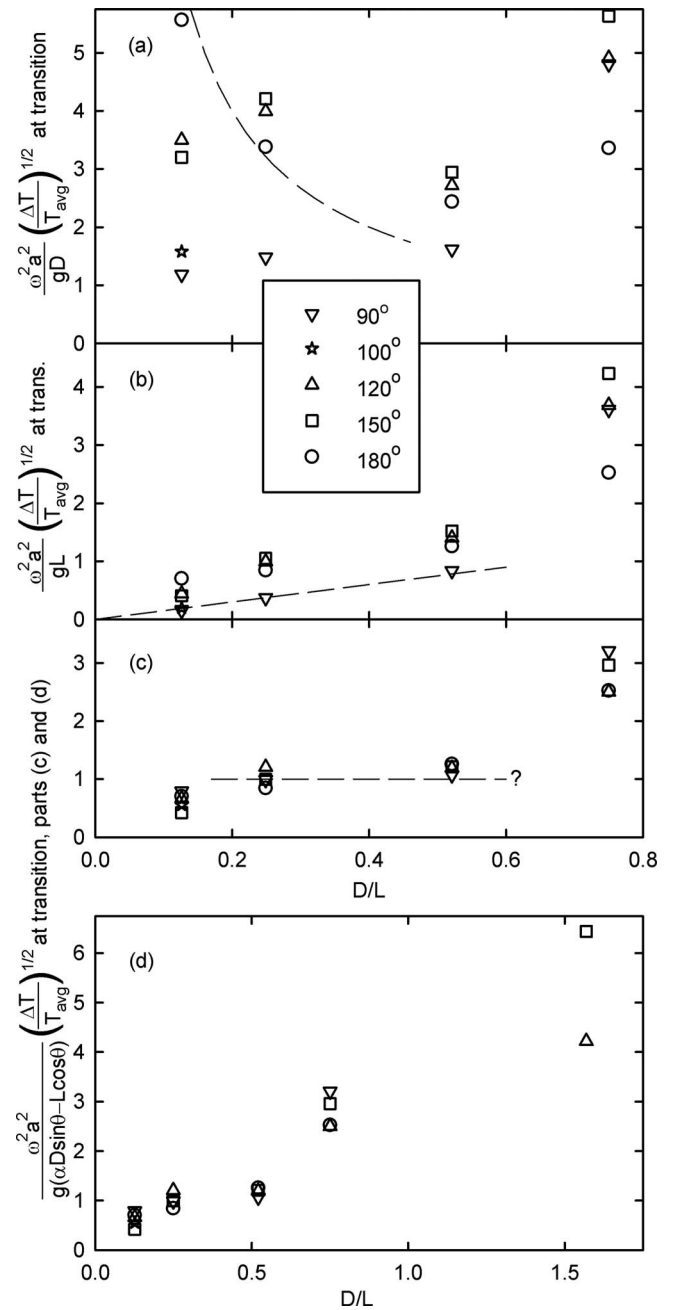


FIG. 7. Transitional values of N_{ptc} based on data from Figs. 4(a) and 6, testing different choices for l in Eq. (20). (a) Choosing $l=D$ yields transitional values of N_{ptc} that are not independent of aspect ratio at small aspect ratio when $\theta \neq 90^\circ$. The dashed curve shows $N_{\text{ptc}} \propto 1/(D/L)$, for comparison with the $\theta=180^\circ$ data. (b) Choosing $l=L$ yields transitional values of N_{ptc} that are more nearly independent of aspect ratio at small aspect ratio when $\theta \neq 90^\circ$, but leaves the $\theta=90^\circ$ data varying almost linearly with aspect ratio, as suggested by the dashed line. (c) Choosing $l=\alpha D \sin \theta - L \cos \theta$, with $\alpha=1.5$, yields transitional values of N_{ptc} that are more nearly independent of both θ and D/L . (d) For completeness, this shows the same data and vertical axis as in (c), but with the data from the highest-aspect-ratio tube included.

because of physics not included in Sec. II: For example, in the $D/L=0.126$ tube, transverse thermal relaxation is faster than in any other tubes, and is comparable to the $\sqrt{l/g}$ convective-motion time, both because the helium-column diameter is smaller and because of the relatively greater contribution of circumferential conduction by the stainless-steel tube wall. A second interpretation would simply discount the

$D/L=0.126$ data because the convection there was weak, differed qualitatively from the other data sets (having no initial rise of \dot{Q} with p_a), and was hard to measure well (e.g., day-to-day and hour-to-hour variations in room temperature would have had a greater effect on this data set than on the others). A third interpretation would be that the analysis of Sec. II is wrong and the data show that $N_{\text{ptc}} \sim c_1 + c_2 D/L$ describes the transition for all D/L , with the data at $D/L=0.52$ to be discounted for some unknown reason.

Resolving these and the other interesting, unanswered questions raised here may require additional experiments, numerical modeling, or both. One important question is whether the suppression of convection depends on the oscillating pressure at all. The time phase difference between the oscillating pressure and oscillating velocity in these experiments was 90° , while practical pulse tubes, transmitting acoustic power, operate closer to a time phase of 0° or 180° , in some cases with the time phase tuned to reduce Rayleigh streaming.¹⁸ Whether this time phase affects the convection suppression, either directly or indirectly through Rayleigh streaming, has not been investigated here. And the magnitude of the oscillating pressure, neglected here in the discussion between Eqs. (20) and (21), might have a significant effect via the gas compressibility, because it makes the oscillating velocity at the ends of the pulse tube different from that in the center.

This situation is most unclear for $D/L > 1$, where Fig. 6(d) shows that the suppression of convection by vibration is very incomplete, or, at best, only partially completed at the amplitudes accessible in this experiment. At such aspect ratios, and with a sometimes a significant fraction of L , ensuring that imperfect flow straightening at the ends of the tube does not affect the measurements may be particularly challenging.

Other well-known rigid-pendulum phenomena, such as parametric resonance and synchronized unidirectional rotation,¹ may also have analogs in pulse tubes, at lower frequencies than those studied here.

ACKNOWLEDGMENTS

This work was supported by license income from thermoacoustic patents at Los Alamos National Laboratory. We thank Robert Keolian and Robert Ecke for many insights about the effects of vibrations on pendula and fluids, and for introductions to the relevant literature.

¹A recent summary and introduction to some of the relevant literature are given by E. I. Butikov, "On the dynamic stabilization of an inverted pendulum," *Am. J. Phys.* **69**, 755–768 (2001).

²L. Blitzer, "Inverted pendulum," *Am. J. Phys.* **33**, 1076–1078 (1965).

³L. D. Landau and E. M. Lifshitz, *Mechanics* (Pergamon, New York, 1960), Sec. 30.

⁴D. Morin, *Introduction to Classical Mechanics* (Cambridge University Press, Cambridge, 2008), Solution 6.5.

⁵R. Radebaugh, "Development of the pulse tube refrigerator as an efficient and reliable cryocooler," Proceedings of the Institute of Refrigeration, London (2000), pp. 11–29; http://cryogenics.nist.gov/Papers/Institute_of_Refrig.pdf (Last viewed 9/30/2009).

⁶G. Thummes, M. Schreiber, R. Landgraf, and C. Heiden, "Convective heat losses in pulse tube coolers: Effect of pulse tube inclination," in *Cryocoolers 9*, edited by R. G. Ross (Plenum, New York, 1997), pp. 393–402.

⁷G. Thummes and L. Yang, "Development of Stirling-type pulse tube coolers driven by commercial linear compressors," in *Infrared Technology and Applications XXVIII*, edited by B. F. Andresen, G. F. Fulop, and M. Strojnik (Society of Photo-Optical Instrumentation Engineering, Seattle, WA, 2003), pp. 1–14.

⁸C. Wang and P. E. Gifford, "A single-stage pulse tube cryocooler for horizontally cooling HTS MRI probe," in *Advances in Cryogenic Engineering: Transactions of the Cryogenic Engineering Conference—CEC*, edited by J. Waynert, J. Barclay, S. Breon, E. Daly, J. Demko, M. DiPirro, J. R. Hull, P. Kelley, P. Kittel, A. Klebaner, J. Lock, J. Maddocks, J. Pfothauer, C. Rey, and Q.-S. Shu (American Institute of Physics, New York, 2004), Vol. **49**, pp. 1805–1811.

⁹S. Backhaus and G. W. Swift, "A thermoacoustic-Stirling heat engine: Detailed study," *J. Acoust. Soc. Am.* **107**, 3148–3166 (2000).

¹⁰D. L. Gardner and G. W. Swift, "A cascade thermoacoustic engine," *J. Acoust. Soc. Am.* **114**, 1905–1919 (2003).

¹¹G. Z. Gershuni and D. V. Lyubimov, *Thermal Vibration Convection* (Wiley, New York, 1998).

¹²G. W. Swift, *Thermoacoustics: A Unifying Perspective for Some Engines and Refrigerators* (Acoustical Society of America, Sewickley, PA, 2002).

¹³G. W. Swift, *Thermoacoustics: A Unifying Perspective for Some Engines and Refrigerators* (Ref. 12), Eq. (7.53).

¹⁴Model C2, Clever Fellows Innovation Consortium, Inc., Troy, NY, <http://qdrive.com> (Last viewed 9/30/2009).

¹⁵Model 8510B-500M37, Endeveco, San Juan Capistrano, CA, www.endeveco.com (Last viewed 9/30/2009).

¹⁶B. Ward, J. Clark, and G. Swift, "Design environment for low-amplitude thermoacoustic energy conversion (DeltaEC)," software and user's guide available from the Los Alamos thermoacoustics web site <http://www.lanl.gov/thermoacoustics/> (Last viewed 9/30/2009).

¹⁷W. M. Rohsenow, J. P. Hartnett, and Y. I. Cho, *Handbook of Heat Transfer* (McGraw-Hill, New York, 1998).

¹⁸J. R. Olson and G. W. Swift, "Acoustic streaming in pulse tube refrigerators: Tapered pulse tubes," *Cryogenics* **37**, 769–776 (1997).

¹⁹K. I. Matveev, S. Backhaus, and G. W. Swift, "The effect of gravity on heat transfer by Rayleigh streaming in pulse tubes and thermal buffer tubes," in *Proceedings of the IMECE 2004: International Mechanical Engineering Congress and Expo*, Fairfield, NJ (American Society of Mechanical Engineers (ASME), New York, 2004), pp. 125–139, Paper No. IMECE 2004-59076.